Model-driven segmentation of X-ray left ventricular angiograms

Oost, C.R.

一心に
‘devotedly’

Chapter 1

Introduction

1.1 Background

Worldwide millions of people suffer from cardiovascular diseases [1;2], which have been the number one cause of death in the western world for decades. Possible defects in the cardiac system can be either blood flow related, electrically induced, or they can be caused by congenital defects of the cardiac anatomy. However, most cardiac defects eventually result in a reduced cardiac function, leading to a reduced blood flow through the body or worse.

The human heart consists of four chambers, the right atrium, the left atrium, the right ventricle and the left ventricle (Figure 1.1). In a healthy subject, deoxygenated blood enters the right atrium and oxygenated blood enters the left atrium from the lungs. When the atria are filled, they contract and the atrio-ventricular valves open, filling both the right and the left ventricle. Subsequently, the atrioventricular valves close, both ventricles contract and the semi-lunar valves open. This way the right ventricle pumps deoxygenated blood to the lungs while the left ventricle pumps oxygenated blood throughout the body.

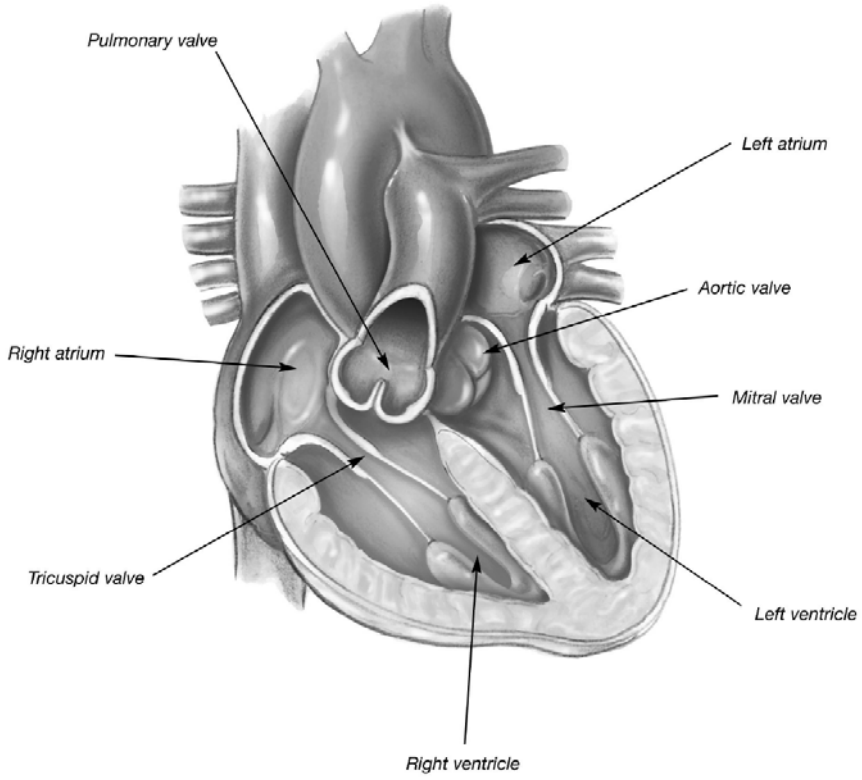

Figure 1.1: A cross section of the human heart (© Edwards Lifesciences, Irvine, California, used with permission).

The process of blood circulation is a delicate rhythmic alternation of contraction and relaxation of the four heart chambers that is regulated by an electrical system, of which the sino-atrial (SA) node is the pacing element. This area of specialized tissue located near the right atrium produces a continuous sequence of electrical pulses, of which the frequency adapts to the metabolic demands of the body. This electrical discharge of the SA-node propagates over the right and the left atria, resulting in a contraction of these chambers, injecting the blood from the atria into the ventricles. The electrical signal then passes through the atrio-ventricular (AV) node to the bundle of His, the right and left bundle and eventually to the Purkinje fibers. This system of electrically conducting fibers causes both the ventricles to contract in a controlled fashion, pumping the blood to the lungs and body.

A variety of cardiovascular diseases exist, which can be roughly categorized as follows. In Ischemic Heart Disease parts of the heart muscle (myocardium) receive a limited supply of blood, resulting in a reduction of cardiac function. One of the main reasons for Ischemic Heart Disease is a narrowing of one or more of the coronary arteries, which supply the myocardium from blood. Such an obstruction can be caused either by an accumulation of plaque in the vessel or by an embolism: a blockage of the vessel by a blood clot. Myocardial Ischemia can eventually lead to the death of myocardial tissue (myocardial infarction).
Arrhythmia is a combinatory term for defects in the electrical cardiac system. Arrhythmia can either be caused by a reduced conductivity, arrhythmical pulse generation by the SA-node, or by ectopic triggers.
Valvular dysfunction can lead to a reduced inflow of blood in a heart chamber or regurgitation through the valve. Common causes of valvular dysfunction are valvular stenoses, valvular inflammation or a congenital valvular defect.
Congestive Heart Failure is a disease that is primarily caused by hypertension, which if left untreated, may cause an irreversible remodeling of the heart due to the increased blood pressure, which in turn reduces cardiac output. It can also be triggered by a (combination of) the aforementioned disorders.

Eventually, most cardiac diseases result in a reduced cardiac function. The large amount of people suffering from cardiac disease stresses the importance of cardiac function diagnostics. Therefore, over time several cardiac imaging methods have been developed that enable the assessment of cardiac function, all with different characteristics. Echocardiography is non-invasive and can give a quick indication of global cardiac function. The image quality however remains relatively poor. Positron Emission Tomography (PET) and Single Photon Emission Computed Tomography (SPECT) are nuclear imaging modalities, in which a radioactive tracer provides information on myocardial perfusion or glucose metabolism in the myocardium (PET), albeit with a relatively low resolution. On the other hand, Magnetic Resonance Imaging (MRI) and Multi Slice Computed Tomography (MSCT) have rapidly evolved over the last decade and are considered to be the modalities of the future. MSCT enables the simultaneous assessment of coronary and ventricular function, and has a high spatial and temporal resolution and a short acquisition time. The main drawback of MSCT is the X-ray radiation dose to which the patient is exposed to. MRI also has a high spatial and temporal

resolution, it does not involve radiation and it has a wide range of possible scan protocols to be applied in order to assess valvular function and ventricular function. The prolonged acquisition time is the major disadvantage of using MRI for functional cardiac imaging. Nonetheless, MSCT and MRI provide a highly intuitive 4 dimensional (3D + time) visualization of the heart.

X-ray LV angiography is also a widely used technique to assess cardiac function. Although this modality gives a 2D or bi-plane visualization of the heart, in the majority of hospitals worldwide a catheterization laboratory (cathlab) with X-ray LV angiography equipment (Figure 1.2) is available. During each cardiac catheterization procedure, the LV angiogram is acquired, providing essential information to the interventional cardiologist, since it enables the analysis of regional and global cardiac function. Drawbacks of X-ray LV angiography are the invasive procedure, the use of contrast dye and, similar to MSCT, the radiation dose to which the patient is exposed. However, due to the availability and a superior spatial and temporal resolution with respect to the MSCT and MRI systems available in the average hospital, X-ray LV angiography is still considered to be an important clinical standard.

The focus of the work presented in this thesis mainly lies on the analysis of X-ray LV angiography, although some chapters also address MRI based studies. The emphasis of the latter studies was mainly on elaborating on conceptual methodology.

Figure 1.2: A cardiovascular X-ray Angiography Imaging Device: The Toshiba CC-i (© Toshiba Cooperation).

1.2 X-ray LV Angiography

1.2.1 X-ray LV Angiography Acquisition

X-ray LV angiography is a catheterization procedure, in which an X-ray opaque contrast dye is injected into the left ventricle through a catheter. This catheter is inserted in the patient's groin, is forwarded through the vascular system of the patient and eventually enters the left ventricle through the aorta. The image acquisition can be performed from two different angles (bi-plane) or from one fixed angle (single-plane). A bi-plane acquisition normally combines the antero-posterior view and the lateral view or the 30° right anterior oblique view and the 60° left anterior oblique view. Although bi-plane image sequences intrinsically provide more information, single-plane acquisitions (generally obtained in the 30° right anterior oblique view) are considered to be the clinical standard.
The amount of injected X-ray opaque contrast dye should be minimized to diminish possible adverse reactions in the patient. When the so-called bolus of contrast fluid arrives at the left ventricle, it fills the ventricle in approximately two or three cardiac cycles. The injection of the contrast agent somewhat irritates the myocardium, causing one or two irregular cardiac contractions (extra-systole). After 8 to 12 cardiac cycles (i.e. approximately 10 seconds) the contrast fluid has been washed out of the left ventricle. The time-window in which the left ventricle is visualized therefore is limited: normally the second or third cardiac cycle after the injection of the contrast dye is considered to provide an optimal visualization, because the distribution of the contrast fluid is maximally homogeneous and possible extra-systole have subsided. From this optimally visualized cardiac cycle two frames are selected for analysis: the end diastolic (ED) image frame, in which the LV volume is maximal, and the first subsequent end systolic (ES) image frame, in which the LV is maximally contracted. An example of a pair of properly acquired ED and ES LV angiogram is shown in Figure 1.3.

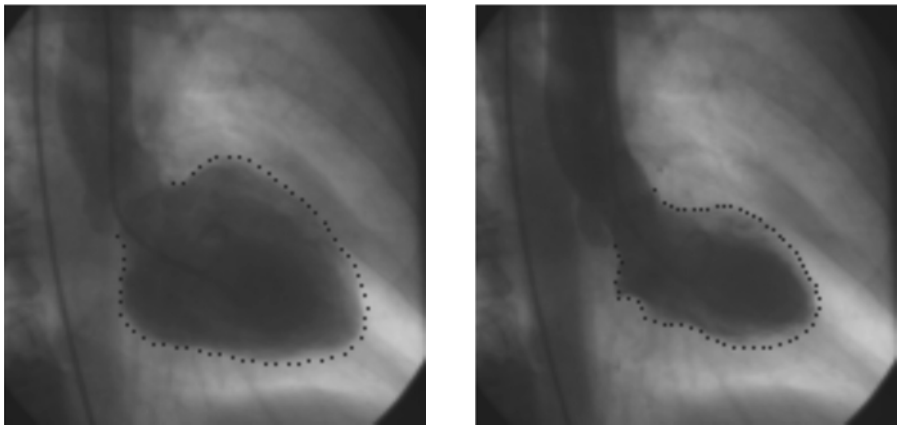

Figure 1.3: ED (left) and ES (right) frame of a properly acquired X-ray angiogram. Black dotted lines denote manually drawn expert contours.

1.2.2 X-ray LV Angiography Image Processing Challenges

The output of an X-ray LV angiography acquisition is an image sequence of approximately 100 to 200 image frames. The clinical information that can be extracted from it is twofold:

- The ejection fraction, defined as the difference between the ED and ES volumes divided by the ED volume.
- The regional myocardial wall motion characteristics.

The acquisition quality of an X-ray LV angiogram can vary a lot, due to the experience of the operator and the physical condition of the patient. For patients it is difficult to comply with the requirement of holding their breath during the acquisition, which is necessary to prevent the diaphragm from overlapping with the posterior wall of the left ventricle. Furthermore, the visualization of the anterior wall can be occluded by a rib. Such overlapping anatomical structures complicate the image interpretation and patient study analysis. Figure 1.4a displays an example of an acquisition in which the LV and the diaphragm are overlapping. Figure 1.4b shows a similar impediment for image interpretation: the shutter of the imaging device, responsible for prevention of over-exposure, can produce a substantial shadow in the image, as expressed in this example as a diagonal dark band.
Poor contrast can be caused by under- or over-exposure of the image sequence, as can be seen in Figure 1.4c. This specific example can be regarded a worst case scenario. Besides under-exposure of the image, the diaphragm and the left ventricle are overlapping and a shutter induced shadow can be observed. Additionally, poor contrast can be caused by the selection of the frames that are to be analyzed by the expert cardiologist. When, for example, the filling of the LV is not optimal because the patient is suffering from dilated cardiomyopathy, or the patient shows a more than average amount of extra-systole after the injection of the contrast fluid, there will be no optimal cardiac cycle to analyze.
During the catheterization procedure, the placement of the catheter tip is of significant importance. The optimal position is in the vicinity of the valve plane, i.e. in the vicinity of the mitral valve (the valve between the left atrium and the left ventricle) and the aortic valve (the valve between the left ventricle and the aorta). When the contrast dye is released it immediately mixes with the incoming blood flow through the mitral valve. Placing the catheter tip near the apex increases the risk of an uneven distribution of the contrast dye, as can be seen in Figure 1.4d.

In current clinical practice there are two ways to interpret an X-ray LV angiographic image sequence. An experienced cardiologist can make a quick estimation of the ejection fraction, just by visual inspection of the image data. In a more thorough analysis the endocardial edge of the left ventricle is delineated manually in the optimally visualized ED and ES frames, using a dedicated software package. Surface areas are calculated from these contour curves and a specialized equation, the area-length method [3] is employed to determine the ED and ES

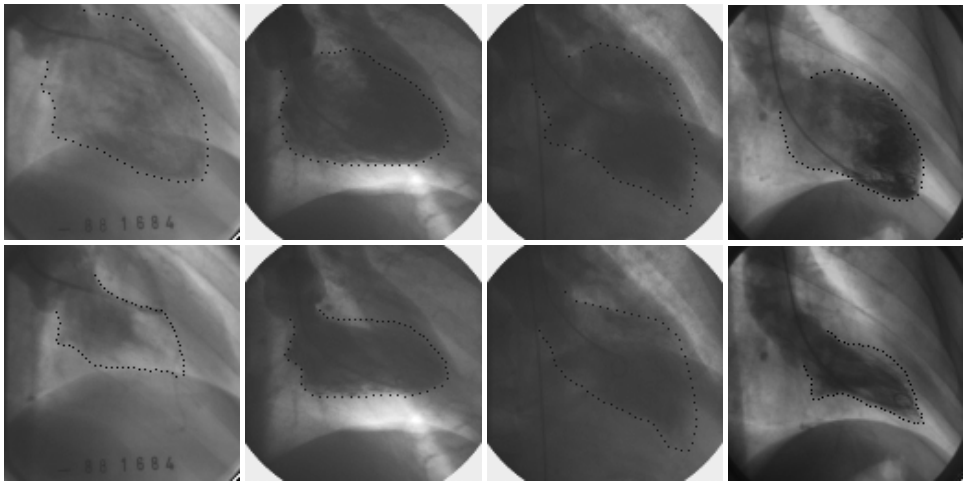

(a) (b) (c) (d)

Figure 1.4: Poor X-ray LV angiogram acquisitions. Upper row displays ED frames, lower row displays ES frames, black dotted lines denote manually traced contours. From left to right: diaphragm overlap, shutter shadow, poor contrast and uneven distribution of contrast agent (mainly observed near the mitral valve in the ED image).

volumes. Subsequently the ejection fraction (EF), defined as the difference between the ED and ES volumes divided by the ED volume, is calculated and regional wall motion can be assessed using a variety of different models [4-6]. Figure 1.5 presents a typical result of such a wall motion model.
Both approaches have serious shortcomings. Visual inspection depends highly on the training of the clinical expert. Moreover, the training culture can differ between different hospitals. Visual inspection is therefore not always reproducible, which leads to a non-standardized diagnosis and which complicates follow-up studies of patients. Manual contouring on the other hand, brings along a high workload. It is time consuming and is prone to inter- and intra-observer variabilities.
Consequently, the need for an automated methodology to assess global cardiac function from X-ray LV angiograms is apparent. It is also clear that, to ensure reproducible results, this automated methodology should provide contours that can be translated into clinical significance: the ejection fraction and the wall motion models.

1.3 Prior Literature on Automated X-ray LV Analysis

For more than three decades attempts have been made to facilitate the delineation of endocardial left ventricular contours in X-ray angiograms [7-18]. The fact that so many researchers have tried to solve this problem underscores the complexity of the problem. Mainly the automatic delineation of the ES image is notoriously difficult. In a properly acquired angiogram one can expect a proper filling and distribution of the contrast dye in the ED frame, making it rather intuitive to decide

on the location of the endocardial border. This does not necessarily hold for the ES image frame, even in a perfectly acquired image sequence. Due to the cardiac contraction, the majority of the mixture of blood and contrast dye is squeezed out of the ventricle, complicating the definition of the endocardial boundary. This specifically holds in the vicinity of trabeculations and papillary muscles (i.e. the muscles restricting the movement of the mitral valve). The amount of contrast fluid in between these structures is generally low, hampering local border detection.

It is generally acknowledged that to achieve an automatic delineation of left ventricular contours, using low level image processing techniques alone do not suffice. Hence the majority of proposed techniques in literature incorporated some level of a priori information, mainly regarding the shape of the left ventricle.

Early examples of automated LV contour delineation methods in angiograms used a priori information regarding general edge characteristics. Chow and Kaneko [7], for example, implemented a dynamic threshold algorithm. Clayton *et al.* [8] determined the left ventricular border positions by calculating edge probabilities. Pope *et al.* [12] applied Dynamic Programming to delineate the left ventricle. Slager *et al.* and Reiber *et al.* [9-11] used a dynamic thresholding based interactive technique that enabled real time (i.e. at video speed being 12.5 to 15 frames/s) processing of a cardiac cinefilm; the thresholds were adapted on a video line-by-line basis. The implemented system, the Contouromat, has been used in many clinical research studies, among others by Hooghoudt *et al.* [19-21].
Tehrani *et al.* [14] proposed one of the first approaches in which a priori information of the shape of the ventricle was used. A statistical model, describing the shape variation of a cardiac left ventricle, was employed to connect fractions of possible LV boundaries, obtained by a low level edge detector. These candidate fractions of the endocardial boundary were either rejected or accepted by a means of a blackboard architecture and the statistical model. Eventually a selection of fractions remained to form a complete LV delineation.
Lilly *et al.* [15] used a similar approach. First a series of low level image processing algorithms (regional intensity information, edge information, and multiple regional thresholding) was used to construct a set of candidate LV edge points. Subsequently Dynamic Programming was applied to fit a contour through these points. Template matching using a template library, derived from manually traced LV contours, incorporated the required a priori information, neutralizing contour irregularities and contour drift due to insufficient image information.
De Figueiredo and Leitão [16] proposed an algorithm based on maximum a priori probability in a Bayesian framework in combination with Markov random field contour modeling. Contrary to the previously described methods, both shape and image intensity information is incorporated in this approach. However, the method was only tested on digital subtraction angiography (DSA), in which an image acquired before the injection of the contrast fluid is subtracted from all following images to suppress the image background. In a clinical setting, optimal background removal is extremely difficult, mainly due to motion artifacts. For many patients it is difficult to hold their breath during the examination, resulting in respiratory motion. Cardiac motion artifacts could be neutralized by ECG gated acquisitions.

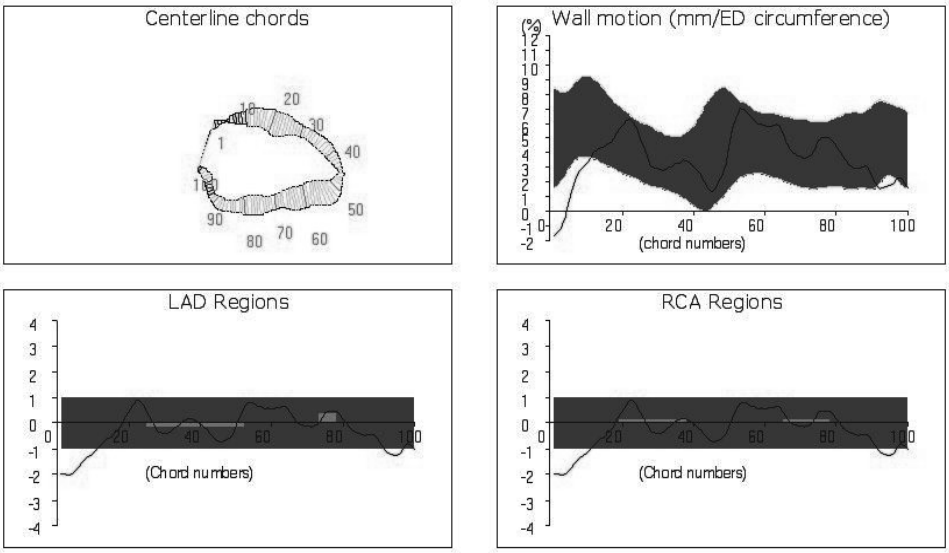

Figure 1.5: Example results from the centerline wall motion model. Top left: ED and ES contour overlay and construction of 100 chords connecting them. Top right: wall motion per chord. Bottom left: wall motion specified for the Left Anterior Descending regions. Bottom right: wall motion specified for the Right Coronary Artery regions.

Nonetheless, using ECG gating for selecting the proper frames for subtraction from the ED and ES images is hampered by arrhythmia caused by the release of the contrast agent or catheter contact with the endocardial wall.
McDonald and Sheehan [17] introduced a method using boosted decision trees for pixel classification based on feature images. Similar to [16], both shape and image intensity information are exploited. This approach mimicked the drawing behavior of the expert cardiologist scrolling through the neighboring time frames around the frame of interest. A clinical expert uses this information to grasp additional information of the contraction dynamics of the left ventricle. The feature images used in McDonald and Sheehan's algorithm were constructed from geometry features and gray-level statistics of such a sequence of images around the ED and ES frames. For initialization of the algorithm, three anatomical landmark points (the endpoints of the aortic valve and the apex) needed to be positioned manually.
Suzuki *et al.* [18] proposed a methodology applying two different edge detection mechanisms: a standard edge detection based on low-pass filtering and edge enhancement and a modified multilayer neural network. The neural network edge detector was trained on manually drawn LV contours and is able to identify less pronounced subjective edges. This approach does not utilize image intensity information and, as in [16], has been applied on DSA images only. After placing the endpoints of the aortic valve manually, the contours are traced automatically.

None of the aforementioned methods has proven to produce left ventricular contours that are of a sufficiently high degree of accuracy and robustness that is acceptable in clinical practice. Only a few of these methods have been introduced in daily clinical practice; van der Zwet *et al.* [13] proposed a method that was

incorporated in a clinical package in the first half of the 1990's. This approach combined a pyramidal segmentation algorithm, neural networks and Dynamic Programming. One general conclusion that can be drawn from this listing of prior work is that automatic delineation of the cardiac left ventricle in X-ray angiograms cannot be achieved without the use of a priori information, describing the shape and appearance of the ventricle. In this work we explore the application of statistical models of shape and appearance to incorporate a priori information into an automatic segmentation scheme for X-ray LV angiograms.

1.4 Statistical Models for Image Segmentation

In the past decade, much progress has been made in the field of automated medical image segmentation. Especially the statistical shape modeling methods introduced by Cootes [22-26] have received widespread attention. Most statistical shape modeling methods consist of two parts: a Point Distribution Model (PDM) that captures object shape and shape variations from a set of examples, and an intensity model that is used for fitting the model to image data. A Point Distribution Model [22] describes the training contours by sampling them with an equal number of corresponding landmark points. After Procrustes alignment [27] of the training shapes to eliminate pose and scale differences, the variations in the shapes are computed using Principal Component Analysis (PCA), an eigenvector decomposition method. A shape similar to the objects in the training set can be generated as a linear combination of the average shape and the modes of variation.

An Active Shape Model (ASM) [23;24] extends the PDM with a model fitting algorithm to segment the object in a target image. Through every point of the PDM a scanline is placed, perpendicular to the contour. Edge information is gathered along these scanlines and used to propose new positions for the contour points. The newly hypothesized shape is expressed as a linear combination of the PDM average and eigenvariations and if any of the modes of variation exceeds a statistical limit (normally 2 or 3 standard deviations), the newly hypothesized shape is constrained to this parameter limit. This way, the generated segmentation hypothesis is constrained to statistically plausible shapes. ASMs have proven their merit in medical image segmentation by combining speed with segmentation robustness. Among many others, examples exist of segmentation algorithms in 2D [28], 2D+time [29] and 3D [30-32].

While in ASMs only the local image intensities along scanlines are used, an Active Appearance Model (AAM) uses an entire image patch to model global image intensity characteristics [25;26]. For every training object an image patch is derived from the object contour. These patches are resampled and aligned and a PCA is applied on the intensities, resulting in an average image intensity representation and a set of eigenvariations. Subsequently, the shape model and the intensity model are concatenated to form a statistical representation of combined shape and intensity. Finally all model and pose parameters are individually perturbed with a

set of known magnitudes, to create a set of pre-computed parameter gradients that can be employed to estimate parameter updates during model matching.
Employing an AAM to segment an object of interest in a target image consists of initializing the model in the vicinity of the object, followed by an iterative matching. The root-mean-square difference between the model and the pixel intensities of the underlying image is minimized with respect to the model and pose parameters using pre-computed parameter gradients. Convergence is achieved when the error does not decrease significantly for a number of iterations. The synthesized model shape represents an approximation of the actual object contour in the image.
Similar to ASMs, the AAM updates are constrained to a certain statistical limit, normally around 2 or 3 standard deviations. Because the parameter gradients that are used to direct the parameter updates are determined individually, every single parameter adjustment attempts to maximally neutralize the difference between the model patch and the underlying image. Hence, parameter updates possibly are overestimated and a statistical constraint is needed.
AAMs implicitly model the relationship between the expert drawn contours and the underlying image features. Hence, AAMs are considered to outperform other approaches, such as ASMs or deformable models because they can cope with images containing fuzzy or spurious edge information.

Application of Active Appearance Models in medical image segmentation are ample and diverse in their extensions. Cootes *et al.* first applied them to knee cartilage segmentation in MRI [25] and later used AAMs for the automatic detection of brain structures in MRI [33]. Another 2D approach was presented by Roberts *et al.* [34], employing a sequence of Active Appearance sub-Models to vertebra segmentation. Beichel *et al.* [35] proposed a robust AAM and applied it to segmentation of hand bones and the segmentation of the diaphragm. In this method the residue, yielded from the subtraction of the model intensities from the image intensities, is used to construct an optimal set of model parameter updates. The first 3D Active Appearance Model, applied to cardiac MRI, was presented by Mitchell *et al.* [36]. Furthermore, Mitchell *et al.* proposed a hybrid AAM/ASM to improve local border delineation in cardiac MRI segmentation [37]. Bosch *et al.* created the Active Appearance Motion Model, modeling a full cardiac cycle of the left ventricle in echocardiography [38]. Another echocardiographic application is presented by Hansegård *et al.* [39], segmenting triplane echocardiograms by a Dynamic Programming constrained AAM. Üzümcü *et al.* explored an AAM in which the shape modeling was performed by using Independent Component Analysis instead of Principal Component Analysis [40]. Finally, Stegmann *et al.* applied an AAM for the registration of cardiac MRI perfusion sequences [41].
This wide range of applications proves the value of AAMs in medical image segmentation. Also for segmentation of the left ventricle in X-ray angiograms, AAMs are expected to perform adequately.

However, some limitations of Active Appearance Models in general and to their application to X-ray LV angiograms specifically can be identified. These shortcomings and their possible solutions will be explored in this thesis, to accomplish a proper segmentation of the left ventricle in X-ray LV angiograms.

1.4.1 Limitations of Active Appearance Models

During matching of an AAM to the underlying image information, the model parameters are iteratively updated. The decision on whether such a new model representation is an improvement or not is based on an error criterion that is defined as the sum of squared differences between the image pixel values and the corresponding model intensity values. Since the error criterion is a global parameter, an AAM does not necessarily emphasize strong local edge information. This can be an advantage when fuzzy or spurious edge information is available in the image. Nonetheless, locally accurate border detection is not guaranteed and in the specific case of X-ray angiography an additional effort is required. Furthermore, as Figure 1.6 illustrates, the error criterion has proven to be unstable when applying an AAM in X-ray LV angiography. Hence, the need for improving the robustness of the algorithm is apparent.

A second limitation is the possible over-constraining towards the training data during statistical model fitting. This can be expressed by a suboptimal local border definition. As reported by Bosch *et al.* [38], an AAM has a tendency to find a "too normal" shape. Furthermore, statistical models of shape (and intensity) are highly dependent on the composition of the training data. For every application it remains difficult to estimate the amount of training data needed and the composition of the characteristics of the training examples.

1.5 Scope of this Thesis

As discussed previously, the interpretation of the ED image in X-ray LV angiography is relatively intuitive, while the ES image is notoriously problematic to segment. However, the ED and ES image frames represent the same left ventricle and the same uptake and washout characteristics of the injected contrast dye. Hence, a high degree of similarity in shape and image intensity information can be observed. This information should be exploited and integrated in the Active Appearance Model.

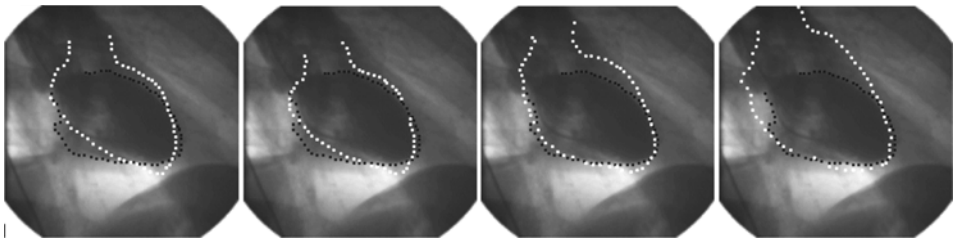

Figure 1.6: An example of spurious error criterion behavior. Black dotted lines denote manually traced reference contours, white dotted lines represent intermediate results obtained by the Active Appearance Model. From Left to right, the error criterion decreases, signifying a supposedly improved model segmentation.

Despite the successful application of AAMs in medical image segmentation, applying them in X-ray LV angiograms remains challenging, due to the limitations described in the previous section. This thesis investigates the application of Active Appearance Models in X-ray LV angiography, to generate an automatic segmentation of the left ventricle in both the ED and the ES phase. The goal of the research described in this thesis is therefore:

- to investigate ways to integrate all available shape and image intensity information in the AAM framework, by exploiting redundancies and similarities between the ED and ES frames.
- to increase the robustness of AAMs with respect to the unstable behavior of the error criterion.
- to investigate the influence of the size and composition of the model training data set on AAM segmentation performance.
- to address the issue of over-constraining towards the training data and investigate ways to improve local LV border delineation.
- to demonstrate the applicability of the resulting algorithm in daily clinical practice, producing clinically acceptable results, reducing the workload of the expert cardiologist and reducing inter- and intra-variabilities in clinical diagnostics.

1.6 Thesis Outline

The remainder of this thesis is structured as follows.

In Chapter 2 an exploratory investigation is reported on the merit of a combined modeling of the ED and ES image frames in an Active Appearance Model framework. For every training example, one shape vector was constructed, concatenating the manually drawn ED and ES contours. Similarly, for all training examples, an image intensity vector was constructed, combining information from both frames. This representation formed the basis of the presented Multi-View Active Appearance Model. In addition, a first step forwards was made towards improving local border delineation. After global segmentation of the left ventricle in ED and ES by the Multi-View AAM, a specialized AAM was employed, focusing on the model description of the LV border. In this specialized model, the intensity information of the center of the ventricle was ignored. Only the intensities in a rim around the LV border were modeled, covering specifically the edge of the ventricle and it's direct surroundings.

The methodology of the Multi-View Active Appearance Model is similar to the Active Appearance Motion Model by Bosch *et al.* [38] in which a full cardiac cycle

was modeled. However, Chapter 3 explored whether this approach could still provide acceptable results when either the amount of data is very sparse in the time domain (only modeling the ED and ES frame in X-ray LV angiography, instead of a full cardiac cycle), or when the shape and intensity features are significantly different for all views. For this latter experiment a Multi-View AAM was constructed to simultaneously model the short-axis view, the two chamber view and the four chamber view of a cardiac MRI acquisition. For both experiments, similarly as in Chapter 2, shape and intensity information of multiple views was modeled in a combined fashion, while the model pose parameters were modeled separately for all views.

Chapter 4 discusses the influence of the composition of the training set that is used in constructing an Active Appearance Model. Due to the problem description, the research goals and the availability of data, this study was performed on a cardiac MRI data set. Three aspects were investigated. First, the optimal size of the training data set, was assessed. In other words, how many training examples are required to obtain a proper statistical description of the population. Second, the ratio between patient study examples and samples from healthy volunteers in the training set was examined. The influence of this ratio on the segmentation results was measured. And third, the influence of the scanner that is used for acquisition was investigated. When segmenting a patient study, acquired with a scanner produced by a specific manufacturer, the segmentation results between applying a scanner specific AAM and an AAM constructed on data from multiple scanners was compared.

In Chapter 5 a new approach to improve local border delineation is presented. To overcome over-constraining of the segmentation result by the model, a dedicated Dynamic Programming is proposed. In this post-processing step, the search area was constrained by the final segmentation result of the Active Appearance Model. Furthermore, the contraction dynamics of the cardiac left ventricle were captured in the Dynamic Programming scheme, by constructing a cost matrix on both the underlying (ED or ES) image information and the information of a subtraction image, created by subtracting the ED frame from the ES frame. A new model matching scheme, the Controlled Gradient Descent, was introduced to improve the robustness of the AAM. In this approach only one or a few model parameters were updated per AAM matching iteration. This way a more smooth and gradual convergence towards the object of interest was expected. In addition, a thorough technical validation was performed, investigating the overall segmentation performance and investigating the merit of all novel elements separately versus their merit when they are applied in a synergetic fashion. Finally, Chapter 5 explored the limits of automation, by comparing a fully automatic X-ray LV angiogram segmentation method with a version of the algorithm in which the user needed to initialize the model by placing three landmark points manually.

Chapter 6 transfers the created methodology into clinical practice. A study on the impact on the clinical workflow was performed, investigating whether the produced contours are of clinically acceptable quality, whether the presented method is capable of reducing the average patient analysis time and the workload of the

cardiologist, and whether the inter- and intra-observer variabilities can be reduced. To assess all this, two expert cardiologists were asked to analyze a data set of 30 patient studies in two ways: First by drawing endocardial contours in ED and ES manually and second by using the automated delineation method, which was incorporated in a dedicated software package. Naturally, in the latter procedure, the expert cardiologists were allowed to edit regions of the automatically determined contours, when they considered them to be sub-optimal. Hence, three types of contours were generated: manual contours, automatic contours and edited automatic contours. These contours were mutually compared with respect to the accuracy of LV delineation. In addition, timings of manual and automatic procedures were compared.

Chapter 7 provides a general discussion and conclusions of the work presented in this thesis.

References

[1] American Heart Association, Heart disease and stroke statistics - 2008 update. Circulation, Dallas, Texas, U.S. Online available: *http://circ.ahajournals.org*

[2] British Heart Foundation Health Promotion Research Group, European cardiovascular disease statistics - 2008 edition. Univ. of Oxford, Oxford, U.K. Online available: *http://www.heartstats.org*

[3] H. Sandler and H. T. Dodge, "The use of single plane angiocardiograms for the calculation of left ventricular volume in man," *American Heart Journal*, vol. 75, no. 3, pp. 325-334, 1968.

[4] C. J. Slager, T. E. H. Hooghoudt, P. W. Serruys, J. C. H. Schuurbiers, J. H. C. Reiber, G. T. Meester, P. D. Verdouw, and P. G. Hugenholtz, "Quantitative assessment of regional left ventricular motion using endocardial landmarks," *Journal of the American College of Cardiology*, vol. 7, no. 2, pp. 317-326, 1986.

[5] E. L. Bolson, S. Kliman, F. Sheehan, and H. T. Dodge, "Left ventricular segmental wall motion: a new method using local direction information," *Computers in Cardiology*, pp. 245-248, 1980.

[6] J. K. Doss, L. D. Hillis, G. Curry, S. E. Lewis, G. J. Dehmer, R. W. Parkey, J. H. Mitchell, and J. T. Willerson, "A new model for the assessment of regional ventricular wall motion," *Radiology*, vol. 143, no. 3, pp. 763-770, 1982.

[7] C. K. Chow and T. Kaneko, "Automatic boundary detection of left ventricle from cineangiograms," *Computers and Biomedical Research*, vol. 5, no. 4, pp. 388-410, 1972.

[8] P. D. Clayton, L. D. Harris, S. R. Rumel, and H. R. Warner, “Left ventricular videometry,” *Computers and Biomedical Research*, vol. 7, no. 4, pp. 369-379, 1974.

[9] C. J. Slager, J. H. C. Reiber, J. C. H. Schuurbiers, and G. T. Meester, “Automated detection of left ventricular contour. Concept and application,” in Heintzen, P. H. and Bursch, J. H. (eds.) *Roentgen-Video-Techniques for dynamic studies of structure and function of the heart and circulation*. Stuttgart: Georg Thieme Publishers, 1978, pp. 158-167.

[10] C. J. Slager, J. H. C. Reiber, J. C. H. Schuurbiers, and G. T. Meester, “Contouromat – A hard-wired left ventricular angio processing system. I. Design and application,” *Computers and Biomedical Research*, vol. 11, no. 5, pp. 491-502, 1978.

[11] J. H. C. Reiber, C. J. Slager, J. C. H. Schuurbiers, and G. T. Meester, “Contouromat – A hard-wired left ventricular angio processing system. II. Performance evaluation,” *Computers and Biomedical Research*, vol. 11, no. 5, pp. 503-523, 1978.

[12] D. L. Pope, D. L. Parker, P. D. Clayton, and D. E. Gustafson, “Left ventricular border recognition using a dynamic search algorithm,” *Radiology*, vol. 155, no. 2, pp. 513-518, 1985.

[13] P. N. J. van der Zwet, G. Koning, and J. H. C. Reiber, “Left ventricular contour detection: a fully automated approach,” *Computers in Cardiology*, pp. 359-362, 1992.

[14] S. Tehrani, T. E. Weymouth, and G. B. J. Mancini, “Model generation and partial matching of left ventricular boundaries,” *Proceedings of SPIE Medical Imaging*, vol. 1445, pp. 434-445, 1991.

[15] P. Lilly, J. Jenkins, and P. Bourdillon, “Automatic contour definition on left ventriculograms by image evidence and a multiple template-based model,” *IEEE Transactions on Medical Imaging*, vol. 8, no. 2, pp. 173-185, 1989.

[16] M. A. T. de Figueiredo and J. M. N. Leitão, “Bayesian estimation of ventricular contours in angiographic images,” *IEEE Transactions on Medical Imaging*, vol. 11, no. 3, pp. 416-429, 1992.

[17] J. A. McDonald and F. H. Sheehan, “Ventriculogram segmentation using boosted decision trees,” *Proceedings of SPIE Medical Imaging*, vol. 5370, pp. 1804-1814, 2004.

[18] K. Suzuki, I. Horiba, N. Sugie, and M. Nanki, “Extraction of left ventricular contours from left ventriculograms by means of a neural edge detector,” *IEEE Transactions on Medical Imaging*, vol. 23, no. 3, pp. 330-339, 2004.

[19] T. E. H. Hooghoudt, C.J. Slager, J.H.C. Reiber, P.W. Serruys, J.C.H. Schuurbiers, and G.T. Meester, "Regional contribution to global ejection fraction used to assess the applicability of a new all motion model to the detection of regional wall motion in patients with asynergy," *PhD thesis, Erasmus University Rotterdam*, 1980.

[20] T. E. H. Hooghoudt, P. W. Serruys, J. H. C. Reiber, C. J. Slager, M. van den Brand, and P. G. Hugenholtz, "The effect of recanalization of the occluded coronary artery in acute myocardial infarction on left ventricular function," *European Heart Journal*, vol. 3, no. 5, pp. 416-421, 1982.

[21] P. W. Serruys, T. E. H. Hooghoudt, J. H. C. Reiber, C. Slager, R. W. Brower, and P. G. Hugenholtz, "Influence of intracoronary nifedipine on left ventricular function, coronary vasomotility, and myocardial oxygen consumption," *British Heart Journal*, vol. 49, no. 5, pp. 427-441, 1983.

[22] T. F. Cootes, C. J. Taylor, D. H. Cooper, and J. Graham. "Training models of shape from sets of examples," *Proceedings of the British Machine Vision Conference*, Berlin: Springer Verlag, 1992, pp. 9-18.

[23] T. F. Cootes and C. J. Taylor, "Active shape models - 'smart snakes'," *Proceedings of the British Machine Vision Conference*, Berlin: Springer Verlag, 1992, pp. 266-275.

[24] T. F. Cootes, C. J. Taylor, D. H. Cooper, and J. Graham, "Active shape models - their training and application," *Computer Vision and Image Understanding*, vol. 61, no. 1, pp. 38-59, 1995.

[25] T. F. Cootes, G. J. Edwards, and C. J. Taylor, "Active appearance models," *Proceedings of the European Conference on Computer Vision*, H. Burkhardt and B. Neumann, Eds., vol. 2, Berlin: Springer Verlag, 1998, pp. 484-498.

[26] T. F. Cootes and C. J. Taylor, "Statistical models of appearance for computer vision," Online available:
http://personalpages.manchester.ac.uk/staff/timothy.f.cootes/Models/app_models.pdf

[27] J. C. Gower, "Generalized procrustes analysis," *Psychometrika*, vol. 40, no. 1, pp. 33-51, 1975.

[28] B. van Ginneken, A. F. Frangi, J. J. Staal, B. M. ter Haar Romeny, and M. A. Viergever, "Active shape model segmentation with optimal features," *IEEE Transactions on Medical Imaging*, vol. 21, no. 8, pp. 924-933, 2002.

[29] G. Hamarneh and T. Gustavsson, "Deformable spatio-temporal shape models: extending active shape models to 2D+time," *Image and Vision Computing*, vol. 22, no. 6, pp. 461-470, 2004.

[30] M. de Bruijne, B. van Ginneken, M. A. Viergever, and W. J. Niessen, "Adapting active shape models for 3D segmentation of tubular structures in medical images," *Proceedings of Information Processing in Medical Imaging,* vol. 2732, Berlin: Springer Verlag, 2003, pp. 136-147.

[31] H. C. van Assen, M. G. Danilouchkine, F. Behloul, H. J. Lamb, R. J. van der Geest, J. H. C. Reiber, and B. P. F. Lelieveldt, "Cardiac LV segmentation using a 3D active shape model driven by fuzzy inference," *Proceedings of Medical Image Computing and Computer-Assisted Intervention*, vol. 2876, Berlin: Springer Verlag, 2003, pp. 533-540.

[32] H. C. van Assen, M. G. Danilouchkine, A. F. Frangi, S. Ordas, J. J. M. Westenberg, J. H. C. Reiber, and B. P. F. Lelieveldt, "SPASM: a 3D-ASM for segmentation of sparse and arbitrarily oriented cardiac MRI data," *Medical Image Analysis*, vol. 10, no. 2, pp. 286-303, 2006.

[33] T. F. Cootes, C. Beeston, G. J. Edwards, and C. J. Taylor, "A unified framework for atlas matching using active appearance models," *Proceedings of Information Processing in Medical Imaging,* vol. 1613, Berlin: Springer Verlag, 1999, pp. 322-333.

[34] M. G. Roberts, T. F. Cootes, and J. E. Adams, "Linking sequences of active appearance sub-models via constraints: an application in automated vertebral morphometry," *Proceedings of the British Machine Vision Conference*, Berlin: Springer Verlag, 2003, pp. 349-358.

[35] R. Beichel, H. Bischof, F. Leberl, and M. Sonka, "Robust active appearance models and their application to medical image analysis," *IEEE Transactions on Medical Imaging*, vol. 24, no. 9, pp. 1151-1169, 2005.

[36] S. C. Mitchell, J. G. Bosch, B. P. F. Lelieveldt, R. J. Van der Geest, J. H. Reiber, and M. Sonka, "3-D active appearance models: segmentation of cardiac MR and ultrasound images," *IEEE Transactions on Medical Imaging*, vol. 21, no. 9, pp. 1167-1178, 2002.

[37] S. C. Mitchell, B. P. F. Lelieveldt, R. J. Van der Geest, H. G. Bosch, J. H. C. Reiber, and M. Sonka, "Multistage hybrid active appearance model matching: segmentation of left and right ventricles in cardiac MR images," *IEEE Transactions on Medical Imaging*, vol. 20, no. 5, pp. 415-423, 2001.

[38] J. G. Bosch, S. C. Mitchell, B. P. F. Lelieveldt, F. Nijland, O. Kamp, M. Sonka, and J. H. C. Reiber, "Automatic segmentation of echocardiographic sequences by active appearance motion models," *IEEE Transactions on Medical Imaging*, vol. 21, no. 11, pp. 1374-1383, 2002.

[39] J. Hansegård, S. Urheim, K. Lunde, and S. I. Rabben, "Constrained active appearance models for segmentation of triplane echocardiograms," *IEEE Transactions on Medical Imaging*, vol. 26, no. 10, pp. 1391-1400, 2007.

[40] M. Üzümcü, A. F. Frangi, M. Sonka, J. H. C. Reiber, and B. P. F. Lelieveldt, "ICA vs. PCA active appearance models: application to cardiac MR segmentation," *Proceedings of Medical Image Computing and Computer-Assisted Intervention*, vol. 2876, Berlin: Springer Verlag, 2003, pp. 451-458.

[41] M. B. Stegmann, H. Olafsdottir, and H. B. W. Larsson, "Unsupervised motion-compensation of multi-slice cardiac perfusion MRI," *Medical Image Analysis*, vol. 9, no. 4, pp.394-410, 2005.